Journal of Applied Electrochemistry (2006) 36:87–96
DOI 10.1007/s10800-005-9026-6

Electrodeposition of Cu from Acidic Sulphate Solutions in the Presence of PEG - Part II Visible Electroreflectance Spectroscopy Measurements during Electrodeposition

B. BOZZINI*, C. MELE and L. D'URZO
Dipartimento di Ingegneria dell'Innovazione, Università di Lecce, via Monteroni, I-73100, Lecce, Italy
*(*author for correspondence, e-mail: benedetto.bozzini@unile.it)*

Received 22 July 2004; accepted in revised form 11 July 2005

Abstract

This paper reports in situ visible electroreflectance measurements carried out during potentiostatic electrodeposition of Cu from acidic sulphate solutions in the absence and presence of PEG. Time-dependent electroreflectance spectroscopy gives information on the evolution of the electronic structure of the growing film, yielding new insight into the electrocrystallisation mode. Roughness effects and purely optical quantities were separated by operating in a suitable range of visible wavelengths. Optical transients were followed with a simple model correlating the relative spectral reflectivity and the degree of dispersion of Cu crystallites. Electroreflectance data were complemented by Raman surface-enhancement measurements and scanning electron microscopy. Electroreflectance results can be correlated with the surface morphology and with the formation of Cu clusters giving rise to different degrees of Raman surface enhancement.

List of symbols

$A(t)$	model function describing the time-dependence of the high-frequency asymptote of the spectral reflectivity curve of coinage metals and alloys
$B(t)$	model function describing the time-dependence of the interband-transition region of the spectral reflectivity of coinage metals and alloys
d	film thickness
$E(\lambda,t)$	purely optical component of the absolute instantaneous reflectivity
f	volume fraction of metallic particles
g_1	purely geometrical factor weighting reflectance
g_2	wavelength-dependent geometrical factor weighting reflectance
i	imaginary unit
$\mathrm{Im}(Z)$	imaginary part of a complex number Z
$R(\lambda,t)$	absolute instanteous spectral reflectance
$Re(Z)$	real part of a complex number Z
t	time
$\Delta R/R(\lambda,t)$	relative instantaneous reflectance
$\Delta\lambda$	model parameter describing the frequency-width of the interband-transition region of the spectral reflectivity of coinage metals and alloys
ε	complex dielectric function
ε_B	dielectric function of bound electrons
ε_c	dielectric function of the composite film
ε_e	dielectric function of the electrolyte
ε_{EM}	dielectric function of the embedding medium
ε_F	dielectric function of free electrons
ε_m	dielectric function of the bulk metal
λ	wavelength
λ_{IB}	interband transition wavelength
λ_n	plasma wavelength of free electrons
λ_{ref}	reference wavelength
$\lambda_{1,2}$	wavelengths set as fixed during ER experiments
$\rho(t)$	roughness at time t
σ	relative instantaneous reflectivity

1. Introduction

1.1. *Cu electrodeposition*

The role of organic additives in Cu electrodeposition from acidic sulphate solutions is critical for recent applications in the fabrication of semiconductors. Notwithstanding intensive investigation, we are still far from a positive understanding of the relevant electrochemical and electrocrystallisation processes. In the first part of this series [1], we reported an electrochemical, Surface-enhanced Raman Spectroscopy (SERS) and Scanning Electron Microscopy (SEM) investigation of the effects of PEG. This paper focuses on *in situ*

electroreflectance measurements, relating them to the effects of PEG on electrocrystallisation processes occurring during potentiostatic electrodeposition. Electroreflectance Spectroscopy (ERS) data are complemented by SEM and are correlated with the potential-dependent surface-enhancement derived from a quantitative analysis of the SERS spectra reported in Part I of this paper [1].

1.2. In situ *VIS reflectance measurements*

The application of in situ VIS electroreflectance in metal electrodeposition studies is expected to yield important information on the electronic and morphological conditions of the growing metal film, and can have prospective applications in on-line process control [2]. Variations of the electrodic spectral reflectance of a metal film undergoing electrochemical deposition can be due to a series of physical reasons, which can be grouped into two broad classes: (i) those unambiguously giving rise to a reflectivity decrease (roughness scattering and surface plasmon excitation [3–6]) in a specific spectral range and (ii) those which can, in principle, give rise to both reflectivity increase or decrease (interfacial compositional effects, alteration of the surface band structure of the metal). ER is typically dominated by the metal surface contribution, especially close to the interband transition. Contributions from the electrolyte portion of the double layer, which have an essentially dielectric character in the relevant energy range, were estimated to be orders of magnitude smaller than the metal surface contribution [7], especially with p-polarisation and low (e.g. 45°) incidence angles.

The optical properties of Cu are known to be extremely sensitive to the sample preparation procedure [8–14]. The spectral reflectivity of Cu is dominated by an interband transition at ca. 450 nm in which energy is adsorbed from the incident light wave to raise an electron into a higher unoccupied state. This transition takes place in addition to the free-electron or Drude adsorption.

2. Experimental

The electrodeposition bath was: $CuSO_4{\cdot}5H_2O$ 20 mM, H_2SO_4 0.5 M. To this solution NaCl 500 ppm and PEG MW 1500, 2 g/L were added. The solutions were prepared from analytic grade chemicals and ultra-pure water with a resistivity of 18.2 MΩ cm. The solutions were degassed by bubbling with nitrogen and by keeping the electrolyte under a nitrogen blanket during the measurements.

Electrochemical measurements were performed with an AMEL 5000 programmable potentiostat. Potential measurements were carried out with an AMEL Ag/AgCl (KCl 3 M) reference electrode; voltages are reported vs. Ag/AgCl. For potentiostatic electrodeposition experiments, wrought brass (90% Cu, 10% Zn, α-phase) cathodes were used, coated with a thick (over 50 mm) layer of X-ray amorphous Ni-P (P 9 %) [15]. The reference electrode probe tip was placed at a distance of ca. 5 mm from the working electrode. The counter electrode was a platinised Ti expanded-mesh electrode exhibiting an area of ca. 10 cm^2.

ERS measurements were made in a cell with a vertical polycrystalline Cu disc working electrode of diameter 5 mm embedded in a Teflon cylindrical holder. A metallographic polishing procedure, consisting of wet grinding with 2400 grit SiC paper, proved adequate for an excellent reproducibility. The counter electrode was a Pt wire loop (1.25 cm^2) concentric and coplanar with the working electrode disc. The reference electrode was placed in a separate compartment, the probe tip was placed 3 mm from the rim of the working electrode disc. An incidence angle of 45°, p-polarised light and a potential modulation frequency of 75 Hz were chosen. The $\Delta R/R$ signal was detected with a lock-in technique. Solid state light sources were employed: a set of three LEDs was used to cover the VIS and UV range ($220 \div 670$ nm). The wavelength was selected with a grating monochromator with a spectral resolution of 7 nm. A photodiode detector was employed.

3. The use of *in situ* spectral electroreflectance spectroscopy for metal electrodeposition studies

Some electroreflectance spectroscopy (ERS) investigations relevant to metal electrochemistry have appeared in the literature, though, to the best of the authors' knowledge, a limited number of such measurements have been carried out during electrodeposition of metal films. Some studies have been published on under potential deposition (UPD) systems and on the progressive coverage of extraneous cathodes with 3D metal layers (see [7, 16] and references contained therein). A theory of the changes in optical properties brought about by the electrodeposition process seems not to be available and we are proposing a first-approximation version in this paper.

During electrodeposition processes, the electrode spectral reflectance (ER) $R(\lambda, t)$ at wavelength λ and time t is, in principle, affected by both electronic and geometrical factors. Variations in the optical properties of the interface and of its roughness are the causes of these two effects. Variations of the optical properties can be caused both by the formation of a compositionally altered surface or by the variation of the electronic structure of the metal, due to the nature of the electrodeposited clusters and crystallites. $R(\lambda, t)$ can thus be written as:

$$R(\lambda, t) = g_1[\rho(t)] \cdot g_2(\lambda) \cdot E(\lambda, t) \quad (1)$$

where $g_1{\cdot}g_2$ is the geometrical factor, which can be shown [3] to be separable into a geometrical factor g_1 – a function of a suitable roughness estimator $\rho(t)$ – and a wavelength-dependent factor g_2. $E(\lambda, t)$ is the electronic contribution. To avoid experimental difficulties in

dealing with absolute reflectance values, it is customary to investigate relative reflectance variations $\Delta R/R$, e.g. [7]. A convenient way to define $[\Delta R/R](\lambda, t)$ is by ratioing $R(\lambda, t)$ to the ER value measured at $t=0$:

$$[\Delta R/R](\lambda, t) = [R(\lambda, t) - R(\lambda, 0)]/R(\lambda, 0) \quad (2)$$

From Equation 1, after some algebra, it results:

$$[\Delta R/R](\lambda, t) + 1 = [g_1(\rho(t)) \cdot E(\lambda, t)]/[g_1(\rho(0)) \cdot E(\lambda, 0)] \quad (3)$$

$[\Delta R/R](\lambda, t)$ is therefore not affected by the spectral dependence of the geometrical factor. The effect of the roughness-dependent component of the geometrical factor can be eliminated by normalising Equation 3 with the $\Delta R/R$ value measured at a reference wavelength λ_{ref}:

$$\sigma(\lambda, t; \lambda_{ref}) = \{[\Delta R/R](\lambda, t) + 1\}/\{[\Delta R/R](\lambda_{ref}, t) + 1\} = [E(\lambda, t) \cdot E(\lambda_{ref}, 0)]/[E(\lambda_{ref}, t) \cdot E(\lambda, 0)] \quad (4)$$

If σ is time-independent no optical contribution is present. A first approximation to the modelling of $\sigma(t)$ transients is possible within the framework of the Maxwell-Garnett theory, predicting the optical properties of films composed of spherical metal clusters embedded into a different medium [17]. In the present case, the embedding medium can be: the electrolyte, organics incorporated at grain boundaries, salt precipitates or metallic crystallites exhibiting a different structure. This theory gives the values of the complex dielectric function of the composite film ε_c as a function of: (i) the dielectric function of the bulk metal ε_m, (ii) the dielectric function of the embedding medium ε_{EM} and (iii) the volume fraction of metallic particles f. If ε_c is used in the expressions for $\Delta R/R$ of [7], one can write $\Delta R/R$ for a given polarisation state as a function of f and λ. In the Appendix we report the deduction of an analytical expression of $[\Delta R/R](f)$ from which $\sigma(f)$ can be derived by use of Equation 4. Some examples of computations of $[\Delta R/R](f)$ referring to Cu clusters in a water matrix (disperse electrodeposit) with bulk Cu as the reference state are shown in Figure 1. In this figure $\Delta R/R$ values are scaled by a known constant factor containing physical constants and the film thickness. In Figure 1 a maximum can be observed for $f<1$. This means that the optical properties of the composite film can yield a higher reflectivity value than for the pure bulk metal. This indeed was found in some of our measurements. The $[\Delta R/R](f)$ functions reported in Figure 1 exhibit an approximately Gaussian shape and the corresponding parameters show a regular wavelength dependence: peak position and full width at half maximum (FWHM), with their 95% confidence intervals, as a function of wavelength, are shown in Figures 2 and 3, respectively. The peak position tends to increase with the wavelength, even though a maximum can be observed at low wavelengths in the visible range. The FWHM regularly decreases with wavelength. Computed normalised $\sigma(f)$ curves is shown in Figure 4. These curves exhibit a maximum / minimum / maximum sequence as the parameter f is varied from 1 to 0; the position of these features changes with the wavelength.

Modelling of the experimental $\sigma(t)$ transients in terms of the electronic properties of the metal undergoing electrodeposition is desirable for both fundamental and applied reasons, such as predicting the electrical resistivity of electrodeposited contacts or rationalising the

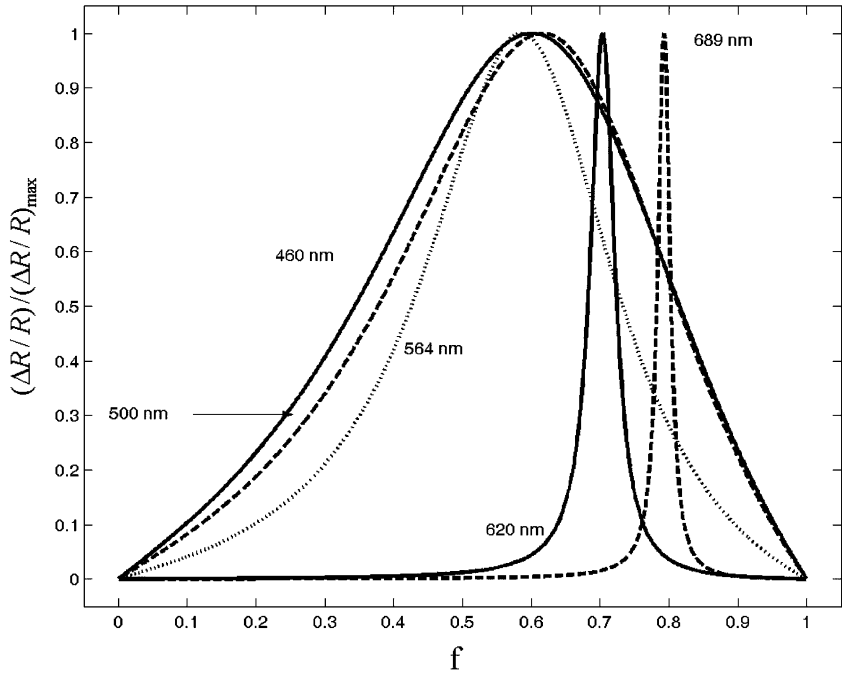

Fig. 1. Normalised computed relative reflectivity ΔR/R as a function of the Cu/water volume fraction f for several wavelengths.

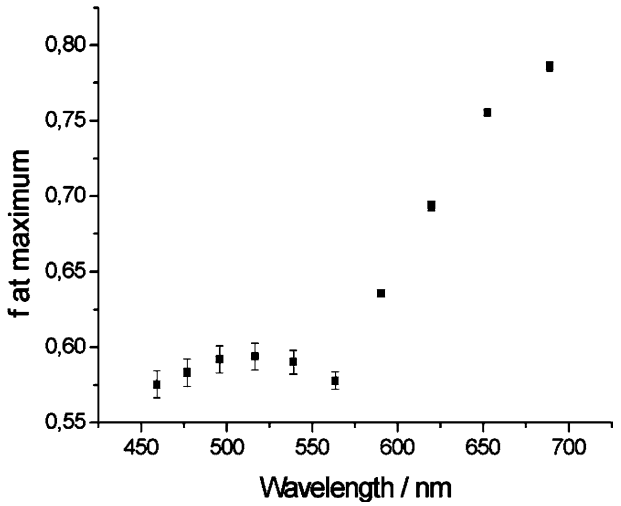

Fig. 2. Peak positions of ΔR/R of ΔR/R vs. f curves (see Figure 1), as a function of wavelength; computed quantities.

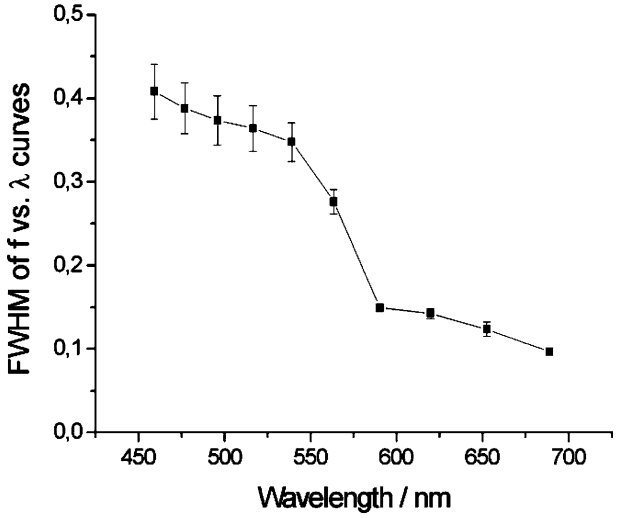

Fig. 3. Full width at half maximum (FWHM) of ΔR/R vs. f curves (see Figure 1), as a function of wavelength; computed quantities.

colour shades of decorative alloy coatings. $[\Delta R/R](\lambda, t)$ is a complicated function of: (i) the complex dielectric function of the metal, (ii) the incidence angle and (iii) the polarisation of the incident radiation. Exact expressions have been derived for some special cases (see, e.g., in [7]). The dielectric function ε of Cu or electrodeposited Cu films, contains sizeable contributions from both free and bound electrons, ε_F and ε_B, respectively: $\varepsilon = \varepsilon_F + \varepsilon_B$. ε can be approximated as (elaborating on [7]):

$$\varepsilon(\lambda, t) \cong 1 - (\lambda/\lambda_n)^2 + i \cdot \mathrm{Im}(\varepsilon_B) \tag{5}$$

λ_n is the plasma wavelength of the free-electrons and i is the imaginary unit. At wavelengths significantly lower than those of the interband transition λ_{IB}, . Equation 5 can be approximated as:

$$\varepsilon(\lambda, t) \cong 1 + i \cdot \alpha \tag{6}$$

where α is a constant. Therefore, for $\lambda << \lambda_{IB}$, $R(\lambda, t) \cong \alpha/(4+\alpha^2) = A$. By fitting experimental data from the literature, it can be assessed that the spectral reflectance of coinage metals can be well approximated with a sigmoidal function of the type:

$$R(\lambda, t) = (1 - A)/\{1 + \exp[(1/\lambda - 1/\lambda_{IB})/\Delta\lambda]\} + A \tag{7}$$

where Δλ is a parameter accounting for the width of the transition. If replicated sets of electrodeposition experiments are run at three suitable wavelengths, some time dependent optical parameters can be evaluated for the process of interest. (i) λ_{ref} can be chosen such that $\lambda_{ref} >> \lambda_{IB}$, hence $E(\lambda_{ref},t) = 1$. (ii) The second wavelength λ_1 is chosen such that $\lambda_1 << \lambda_{IB}$, hence $E(\lambda_1, t) = A(t)$ (iii) The third wavelength is set at $\lambda_2 \cong \lambda_{IB}$, hence:

$$E(\lambda_2 - \lambda_{IB}) \cong 1/2 \cdot [1 + A(t)] - [1/\lambda_2 - 1/\lambda_{IB}(t)] \cdot [\mathrm{A(t)} - 1]/[4 \cdot \Delta\lambda(t)]. \tag{8}$$

For ease of notation, we define the function $B(\lambda, t) = [1/\lambda_2 - 1/\lambda_{IB}(t)]/\Delta\lambda(t)]$.

By using Equation 7, Equation 4 can be rewritten as:

$$\sigma(\lambda_1, t; \lambda_{ref}) = A(t)/A(0) \tag{9}$$

and

$$\sigma(\lambda_2, t; \lambda_{ref}) = 1/2 \cdot [A(t) + 1] - 1/4 \cdot [A(t) - 1]B(\lambda, t) \tag{10}$$

From a set of potentiostatic experiments carried out at three selected wavelengths, one can therefore estimate the following time- and potential-dependent quantities: $A(t,V)$ and $B(t,V) = [1/\lambda_2 - 1/\lambda_{IB}(t, V)]/\Delta\lambda(t, V)$. The former describes the variation of the high-frequency absorbing part of the complex dielectric function and the latter the variation of the band structure related to the interband transition.

4. Results and discussion

4.1. *Electroreflectance Spectroscopy*

Reflectivity transients were recorded under potentiostatic conditions at three wavelengths: 460, 500 and 620 nm without and with PEG. No obvious order appears in the curves observed: both increasing and decreasing time variations are found and the sequence of the transients with electrodeposition potentials depends on the wavelength of the incident light and on the bath chemistry. The increase of reflectivity observed in most curves, and in all cases in the presence of PEG, can be directly related to variations of electronic properties. The $[\Delta R/R](\lambda,t)$ transients were corrected for roughness contributions by normalising the data measured at $\lambda = 460$ and 500 nm by those recorded at $\lambda_{ref} = 620$ nm – where the spectral reflectivity is close to 100% -, thus obtaining the $\sigma(t;\lambda;\lambda_{ref})$ curves, reported in Figures 5, 6 and 7, 8 for PEG-free and PEG-containing systems, respectively.

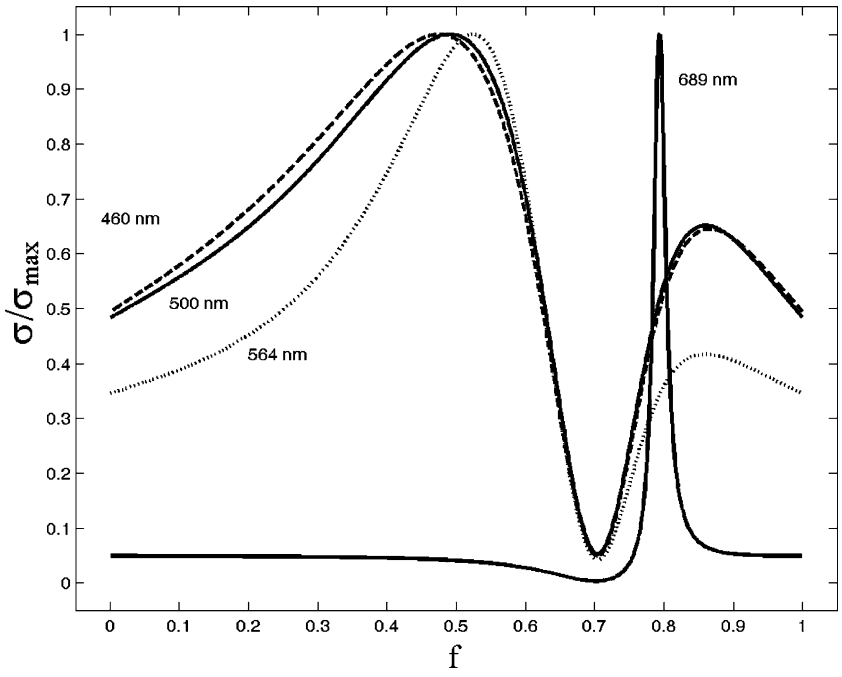

Fig. 4. Normalised σ(f) curves (see text) as a function of the Cu/water volume fraction f for several wavelengths.

$\sigma(t;\lambda;\lambda_{ref})$ transients can be interpreted in terms of the Maxwell-Garnett theory, as detailed above. $\sigma(f)$ curves can be computed by Equation 4 from $[\Delta R/R](f,\lambda)$. According to the theoretical $\sigma(f)$ curves shown in Figure 4, an increase in f can be interpreted as positively correlated with the defect density present in the electrodeposited film; the latter quantity can, in turn, be associated with the degree of irreversibility, and hence the cathodic overvoltage, of the electrodeposition process. Our results are summarised in Table 1. The trends observed in the experimental transients can be correlated with the $\sigma(f;\lambda)$ curves shown in Figure 4. In general, the behaviour noticed at increasing overvoltages can be related to that at increasing f values, for f values in the ranges ca. $0.85 \rightarrow 0.475$ and ca. $0.85 \rightarrow 0.525$ for the systems without and with PEG, respectively. Within a given bath, the differences in trends can be explained in terms of the wavelength-dependence of the maxima and minima of the $\sigma(f)$ curves. Between baths, one can observe that the differences in behaviour between the solutions without and with PEG can be described in terms of lower f values for the latter system: this can correlate to the higher growth stability observed in the presence of the additive [1].

Experimental $\sigma(t;\lambda)$ transients were also elaborated in order to extract the reflectivity parameters $A(t)$ and $B(t)$, as described above. Since $A(t)$ is directly proportional to $\sigma(t,\ 460\ \text{nm},\lambda_{ref})$, we do not plot these

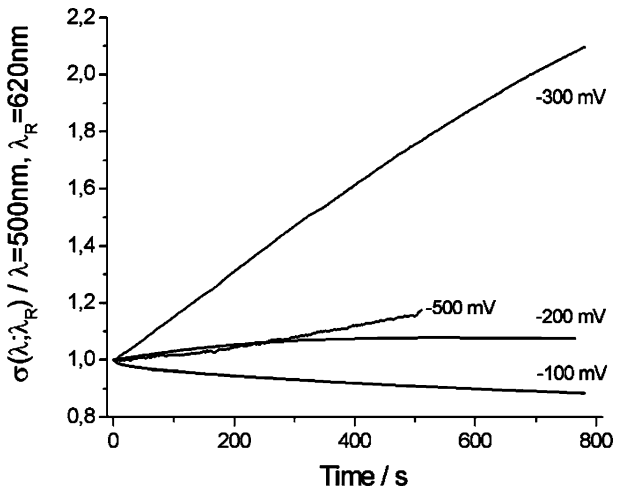

Fig. 5. Experimental optical relative reflectivity transients σ(t) (see text), current wavelength $\lambda = 500$ nm, reference wavelength $\lambda_{ref} = 620$ nm: Cu bath without PEG, potentiostatic electrodeposition at the voltages shown (vs. Ag/AgCl).

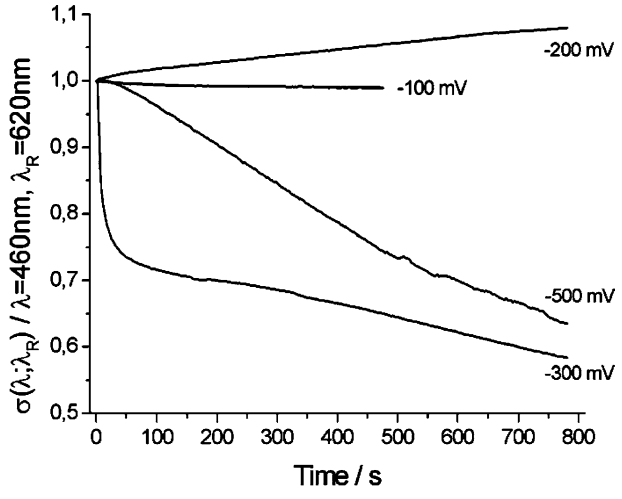

Fig. 6. Experimental optical relative reflectivity transients σ(t) (see text), current wavelength $\lambda = 460$ nm, reference wavelength $\lambda_{ref} = 620$ nm: Cu bath without PEG, potentiostatic electrodeposition at the voltages shown (vs. Ag/AgCl).

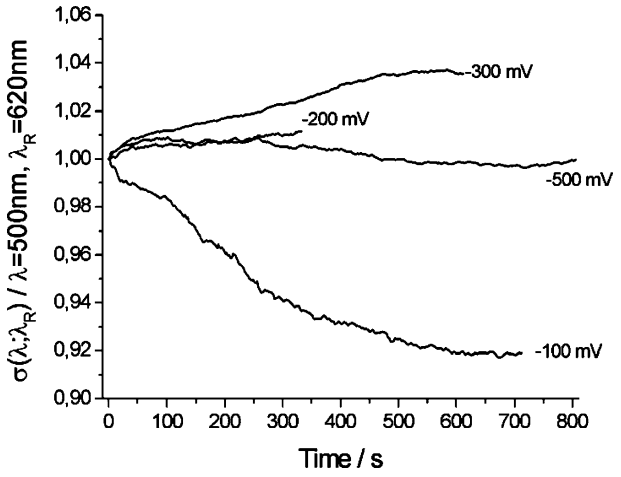

Fig. 7. Experimental optical relative reflectivity transients $\sigma(t)$ (see text), current wavelength $\lambda = 500$ nm, reference wavelength $\lambda_{ref} = 620$ nm: Cu bath with PEG, potentiostatic electrodeposition at the voltages shown (vs. Ag/AgCl).

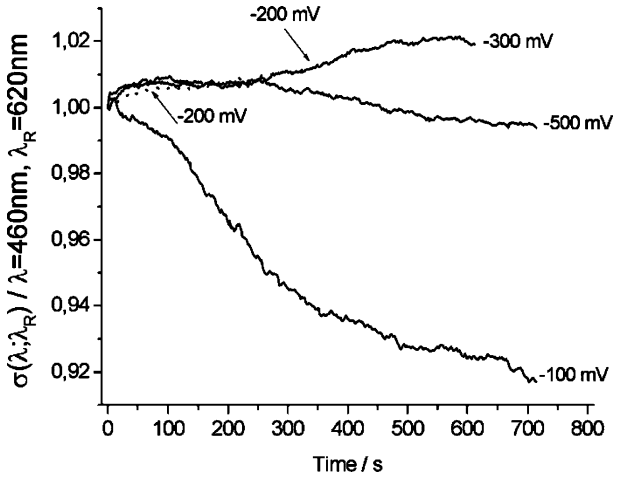

Fig. 8. Experimental optical relative reflectivity transients $\sigma(t)$ (see text), current wavelength $\lambda = 460$ nm, reference wavelength $\lambda_{ref} = 620$ nm: Cu bath with PEG, potentiostatic electrodeposition at the voltages shown (vs. Ag/AgCl).

Table 1. Qualitative description of the slopes of the $\sigma(t,\lambda;\lambda_{ref})$ transients, with $\lambda_R = 620$ nm. One arrow indicates a mild slope, two arrows a stronger one

Bath	Wavelength λ nm	−100 mV	−200 mV	−300 mV	−500 mV
No PEG	460	↓	↑	↑↑	↑
No PEG	500	↓	↑	↓↓	↓↓
With PEG	460	↓	↑	↑	↑
With PEG	500	↓	↑	↑	↓

transients separately, but refer to Figures 5 and 7 for the solution without and with PEG, respectively. $B(t)$ transients for PEG-free and PEG-containing baths are shown in Figures 9 and 10, respectively. The qualitative trends of the experimental $B(t)$ curves as a function of bath composition and cathodic potential are summarised in Table 2. A plot showing computed normalised $A(f)$ and $B(f)$ curves is reported in Figure 11. By construction, $A(f)$ shows the same f dependence as the lower-wavelength $\sigma(f)$ curves and the same comments apply. From Table 2 and Figure 11 it can be noticed that the potential-dependent trends of the experimental $B(t)$ curves for the two baths, as the potential is shifted in the cathodic direction, show a reasonable agreement with the behaviour of the computed $B(f)$ curve when the f parameter is decreased starting from a value of ca. 0.85. In particular, on decreasing f, the sharp maximum of the $B(f)$ curve seems to be passed by the experimental $B(t)$ transients measured at −300 and −500 mV in the absence of PEG and only at −500 mV in the presence of the additive. Again, the association of lower f values to the PEG-containing solution under otherwise identical

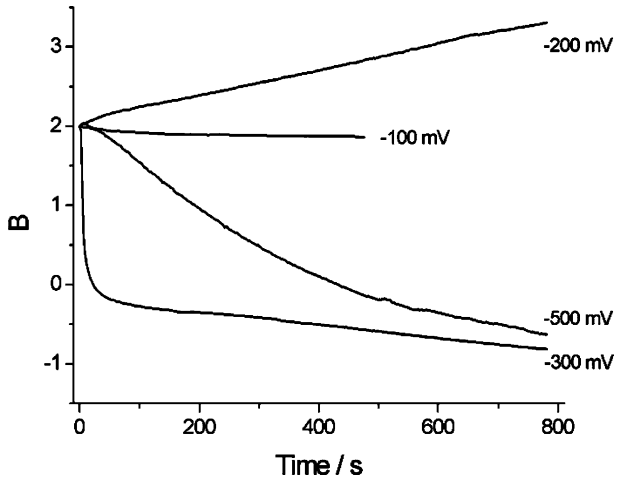

Fig. 9. Experimental B(t) transients (see text): Cu bath without PEG, potentiostatic electrodeposition at the voltages shown (vs. Ag/AgCl).

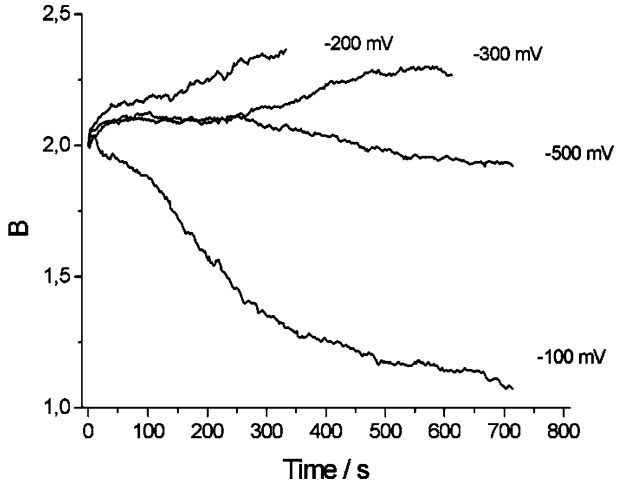

Fig. 10. Experimental B(t) transients (see text): Cu bath with PEG, potentiostatic electrodeposition at the voltages shown (vs. Ag/AgCl).

Table 2. Qualitative description of the slopes of the B(t) transients

Bath	−100 mV	−200 mV	−300 mV	−500 mV
No PEG	↓	↑	↓↓	↓↓
With PEG	↓	↑	↑	↓

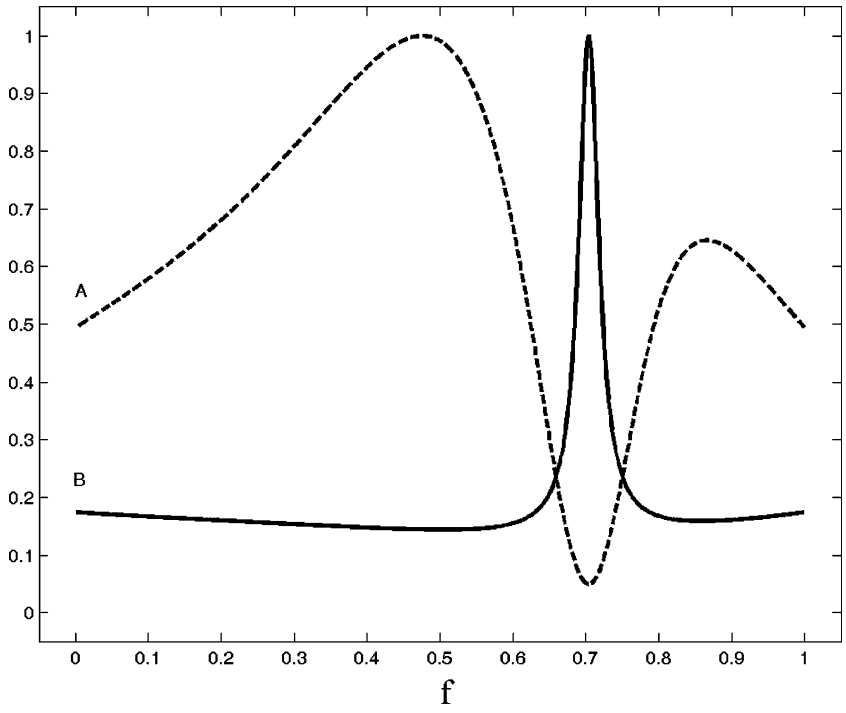

Fig. 11. Computed A and B optical parameters (see text) as a a function of the Cu/water volume fraction *f*.

operating conditions can be explained with a higher perfection of the deposits obtained from the additive-containing bath.

4.2. *SERS Background*

In SERS also the background is known to undergo surface enhancement. Physical reasons for this fact are still an open problem (see, e.g., [18–21] for relevant reviews). In the literature several explanations have been put forward for this phenomenon, such as: (i) adatom-substrate interactions [22–24], (ii) charge-carrier excitations [25], (iii) surface electronic states due to chemisorption bonds [26] or (iv) adsorbed carbon impurities [27–32]. A combination of causes (i), (iii) and (iv) has also been considered [33]. SERS enhancement of the background can be unambiguously distinguished from fluorescence [34]. Whatever the origin of surface enhancement, since this is unambiguously related to the existence of suitable metal surface morphologies and to the presence of some surface species, systematic variations of SERS background intensity under otherwise identical conditions can be used as a diagnostic tool of the surface conditions, that, in turn, are associated to both electronic-structure and roughness variations of the electrodeposited film.

In the present research, we obtain a SERS background of the continuum type (e.g. [26]). We evaluate the potential-dependent SERS background. The potential variations of the SERS background at 1300 and 2000 cm^{-1} are shown in Figure 12. The same trends of the background intensity with electrodeposition potential can be noticed at both investigated Raman shifts. The PEG-free system exhibits a limited potential-dependence of the background intensity, anticorrelated with the cathodic polarisation; a relatively more marked decrease is found in the presence of PEG. One can conclude that the formation of SERS active features in the presence of PEG spans a larger range of conditions in comparison with the PEG-free bath. This behaviour might relate to the effects of PEG on the cathodic charge-transfer mechanism, reported in [1]. Higher absolute values of the SERS background intensity in the presence of PEG can be related to the grain-refining action of the suppressor.

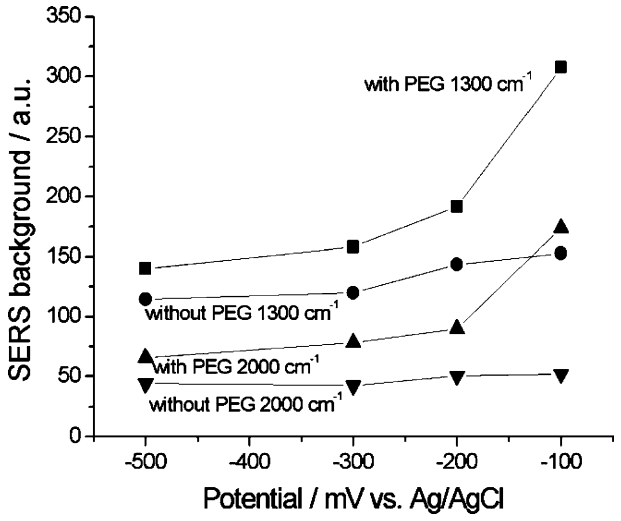

Fig. 12. SERS background at 1300 and 2000 cm^{-1} as a function of potentiostatic electrodeposition voltage (vs. Ag/AgCl) for Cu baths without and with PEG.

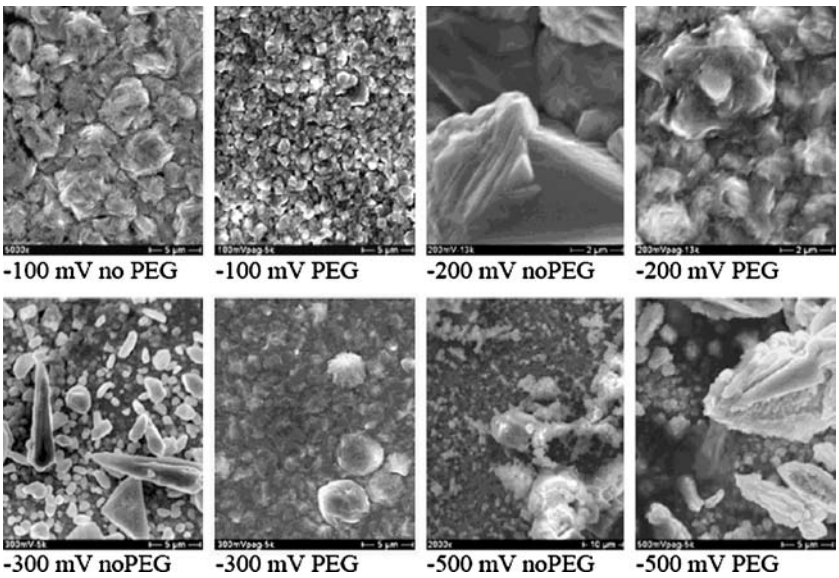

Fig. 13. SEM micrographs of Cu layers obtained by potentiostatic electrodeposition at the voltages indicated (vs. Ag/AgCl) for 500 s from baths without and with PEG.

4.3. *Scanning Electron Microscopy*

The morphological variations corresponding to potentiostatic electrodeposition for 500 s at −100, −200, −300 and −500 mV in the absence and in the presence of PEG were examined by SEM (Figure 13). The morphological effects of potential and PEG are consistent with the ER transients and their morphological interpretation in terms of roughening and degree of deposit compaction. In the absence of the organic additive, on increasing the cathodic voltage one can notice that compact granular deposits are grown at −100 and −200 mV, with larger grains at the higher cathodic polarisation; dendritic growth sets in at −300 mV and loose and powdery Cu is formed at −500 mV. Grain refining and stabilising activity of PEG can be recognised. Granular growth is observed up to −300 mV, the onset of dendritic growth seems to be delayed to −500 mV.

5. Conclusions

In this research we analysed the potentiostatic growth process of Cu from acidic sulphate solutions without and with added PEG by an in situ optical method. Electroreflectance transients were measured during electrodeposition at various visible wavelengths. A suitable data treatment procedure allows electronic information to be extracted from the measured reflectivity. The main effect of the addition of PEG is that electroreflectance tends to increase at all investigated potentials. This behaviour can be modelled with a higher degree of compactness of the granular electrodeposited Cu layers, related to the smoothing action of PEG proved by SEM. The SERS enhancement of the background shows higher values and larger potential dependence for the PEG-containing system, suggesting an increased nucleation activity. This behaviour is coherent with both electroreflectance and SEM results, hinting at the fact that finer-grained, more compact Cu layers tend to grow from the electrolyte containing the polymeric suppressor under otherwise identical electrochemical conditions.

Acknowledgements

This research is part of the "Cathodic Accretion Ruled by Layer Adsorption" Project of the Faculty of Engineering, Lecce University. Expert assistance with electrochemical and spectroelectrochemical experiments is gratefully acknowledged to Mr. Francesco Bogani.

Appendix

Let E(λ, t) describe the purely optical properties of the three-phase planar system discussed in [7]; the relative instantaneous reflectance [$\Delta R/R$](λ, t) is expressed by Equation 3. [$\Delta R/R$](λ, t) can be interpreted in terms of the time-dependent optical properties of the layer being electrodeposited. According to [7], for parallel polarisation, one can write:

$$\Delta R/R(\lambda,t) = 8\sqrt{2\pi}\mathrm{d}\sqrt{\varepsilon_\mathrm{e}}/\lambda \cdot \mathrm{Im}\{[(\varepsilon_\mathrm{c}-\varepsilon_\mathrm{m})/(\varepsilon_\mathrm{e}-\varepsilon_\mathrm{m})] \cdot [(1-0.5\cdot\varepsilon_\mathrm{e}/(\varepsilon_\mathrm{c}\varepsilon_\mathrm{m})\cdot(\varepsilon\mathrm{c}+\varepsilon_\mathrm{m}))/(1-0.5 \cdot(\varepsilon_\mathrm{e}+\varepsilon_\mathrm{m})/\varepsilon_\mathrm{m})]\} \quad (A1)$$

where d is the electrodeposited film thickness. Equation A1 provides a physical interpretation of the ratio $E(\lambda, t)/E(\lambda,0)$ present in Equation 3 in terms of complex dielectric functions, within the framework of the linear three-phase model of [7]. The separation of the geometrical and optical components of the observed reflectivity

is achieved by normalising Equation 3, measured at a given wavelength λ to that measured at a reference wavelength λ_{ref}. $E(\lambda,0)$ and $E(\lambda_{ref},0)$ are quantities known from tabulations of the dielectric functions of the bulk metal ε_m and of the electrolyte ε_e, since at $t=0$ the optically-affected interfacial film has not formed yet.

In this work, we treat the time-dependence of $\Delta R/R(\lambda, t)$ in the framework of the Maxwell-Garnett theory ([7, 17]). 3D electrochemical metal growth gives rise to the simultaneous formation of independent crystallites, eventually leading to the formation of layers with different degrees of continuity. Discontinuous metal films exhibit optical properties that are different from those of bulk metal, owing to both clustering effects and presence of an embedding medium with a different dielectric constant. In the first-approximation case of: (i) spherical metal clusters, (ii) metal clusters displaying the same optical properties as the bulk metal and (iii) embedding medium with a purely real dielectric constant (such as water), the Maxwell-Garnett equation yielding the complex dielectric constant of the composite medium $Re(\varepsilon_c)+\mathrm{i}\cdot\mathrm{Im}(\varepsilon_c)$ is:

$$(Re(\varepsilon_c)-1+i\cdot\mathrm{Im}(\varepsilon_c))/(Re(\varepsilon_c)+2+\mathrm{i}\cdot\mathrm{Im}(\varepsilon_c)) = f\cdot(Re(\varepsilon_m)-1+\mathrm{i}\cdot\mathrm{Im}(\varepsilon_m))/(Re(\varepsilon_m)+2+\mathrm{i}\cdot\mathrm{Im}(\varepsilon_m))+(1-f)\cdot(\varepsilon_{EM}-1)/(\varepsilon_{EM}+2) \quad (A2)$$

where c stands for "composite", m for "metal" and EM for "embedding medium", f is the volume fraction of metal in the composite material.

After some algebra, $Re(\varepsilon_c)$ and $\mathrm{Im}(\varepsilon_c)$ can be rewritten:

$$Re(\varepsilon_c) = 3\cdot(1-Re(A))/[(\mathrm{Im(A)})^2+(1-Re(A))^2]-2 \quad (A3.1)$$

$$\mathrm{Im}(\varepsilon_c) = 3\cdot\mathrm{Im(A)}/[(\mathrm{Im(A)})^2+(1-\mathrm{Re(A)})^2] \quad (A3.2)$$

where:

$$Re(A) = f\cdot\{[(Re(\varepsilon_m)-1)\cdot(Re(\varepsilon)+2)+(\mathrm{Im}(\varepsilon))^2]/[(Re(\varepsilon))^2+(\mathrm{Im}(\varepsilon))^2]\}+(1-f)\cdot(\varepsilon-1)/(\varepsilon_e+2) \quad (A4)$$

and

$$\mathrm{Im(A)} = 3\cdot f\cdot\mathrm{Im}(\varepsilon_m)/[(Re(\varepsilon_m)+2)^2+(\mathrm{Im}(\varepsilon_m))^2] \quad (A5)$$

Once the complex dielectric constant of the composite electrodeposited layer is known, one can compute the spectral reflectivity of the substrate-layer-electrolyte system. In the case of ERS, a convenient way to do this is to represent the relative spectral reflectivity as the ratio of the reflectivities of the systems in the absence and in the presence of the composite layer (i.e. the bulk-Cu/electrolyte and the bulk-Cu/electrodeposited-Cu/electrolyte interfaces, respectively). This can be done e.g. with the linearised three-layer approach of [7, 16], yielding for the parallel polarised light and incidence angle at 45° the following expression:

$$\Delta R/R = 4\pi\mathrm{d}(2\cdot\varepsilon_{EM})^{1/2}/\lambda\cdot\mathrm{Im}(\beta_1\cdot\beta_2/\beta_3) \quad (A6.1)$$

where:

$$\beta_1 = [Re(\varepsilon_c)-Re(\varepsilon_m)+\mathrm{i}\cdot(\mathrm{Im}(\varepsilon_c)-\mathrm{Im}(\varepsilon_m))]/[\varepsilon_{EM}-Re(\varepsilon)+\mathrm{i}\cdot\mathrm{Im}(\varepsilon_m)] \quad (A6.2)$$

$$\beta_2 = 1-\varepsilon_{EM}/2\cdot[Re(\varepsilon_c)+Re(\varepsilon_m)+\mathrm{i}\cdot(\mathrm{Im}(\varepsilon_c)+\mathrm{Im}(\varepsilon_m))]/[(Re(\varepsilon_c)+\mathrm{i}\cdot\mathrm{Im}(\varepsilon_c))\cdot(Re(\varepsilon_m)+\mathrm{i}\cdot\mathrm{Im}(\varepsilon_m))] \quad (A6.3)$$

$$\beta_3 = 1-1/2\cdot(\varepsilon_{EM}+Re(\varepsilon_m)+\mathrm{i}\cdot\mathrm{Im}(\varepsilon_m))/(Re(\varepsilon_m)+\mathrm{i}\cdot\mathrm{Im}(\varepsilon_m)) \quad (A6.4)$$

References

1. B. Bozzini, C. Mele, L. D'Urzo, G. Giovannelli and S. Natali. 'Electrodeposition of Cu from Acidic Sulphate Solutions in the Presence of PEG: An Electrochemical and Spectroelectrochemical Investigation - Part I'. *J. Appl. Electrochem*, accepted.
2. B. Bozzini, L. Corradini, C. Lenardi, C. Mele and M. Serra. 'Feedback control of morphology evolution in metal electrodeposition by optical means'. Proc. 199th Electrochemical Society Meeting, 25–29/03/2001 Washington DC.
3. J.M. Elson, H.E. Bennett and J.M. Bennett. *in* R.R. Shannon and J.C. Wyant (Eds), 'Applied Optics and Optical Engineering' vol. vii, (Academic Press, New York, 1979) pp. 199–208.
4. H. Raeter. *in* V.M. Agranovic and D.L. Mills (Eds), 'Surface Polaritons', (North-Holland, Amsterdam, 1982), p. 331.
5. D.M. Kolb and R. Kötz, *Surf. Sci.* **64** (1977) 96.
6. R. Kötz and D.M. Kolb, *Z. Phys. Chem. Neue Folge* **112** (1978) 69.
7. D.M. Kolb, *in* R.J. Gale (Ed.), 'Spectroelectrochemistry', (Plenum Press, N.Y., 1988), (a) pp. 87–188.
8. S. Roberts, *Phys. Rev.* **118** (1960) 1509.
9. G.P. Pells and M. Shiga, *Proc. Phys. Soc., London (Solid State Phys.)* **2** (1969) 1835.
10. P.O. Nilsson, *Pyhs. Scripta* **1** (1970) 189.
11. H. Bispinck, *Z. Naturforsch* **A25** (1970) 70.
12. H.G. Liljenvall, A.G. Mathewson and H.P. Myers, *Phil. Mag. VIII* **22** (1970) 243.
13. A.G. Mathewson and H.P. Myers, *J. Phys.* **F2** (1972) 403.
14. O. Hunderi, *Phys. Rev. B* **7** (1973) 3419.
15. B. Bozzini, P.L. Cavallotti, M. Ivanov, L. Arras, S. Garbarino, E. Terrenzio and P. Visigalli, *IEEE Trans. Magn.* **26** (1990) 45.
16. D.M. Kolb. *in* H. Gerischer and C.W. Tobias (Eds), Advances in Electrochemistry and Electrochemical Engineering Vol. 11, (J. Wiley & Sons, NY, 1978), p. 125.
17. O.S. Heavens, *Optical Properties of Thin Solid Films* (Dover, N.Y., 1991), pp. 177–180.
18. T.E. Furtak and J. Reyes, *Surf. Sci.* **93** (1980) 351.
19. A. Otto, *Indian J. Phys.* **77B** (2003) 63.
20. M. Moskovits, *Rev. Mod. Phys.* **57** (1985) 783.
21. R.L. Birke, T. Lu and J.R. Lombardi. *in* R. Varma and J.R. Selman (Eds), "Techniques for Characterization of Electrodes and Electrochemical Processes", (J. Wiley & Sons, NY, 1991), p. 211.
22. J. Billmann, G. Kovatcs and A. Otto, *Surf. Sci.* **92** (1980) 153.
23. A. Otto, *Surf. Sci.* **75** (1978) L392.
24. A. Otto, J. Timper, J. Billmann and I. Pockrand, *Phys. Rev. Lett.* **45** (1980) 46.

25. C.Y. Chen, E. Burstein and S. Lundquist, *Solid State Comm.* **32** (1979) 63.
26. R.L. Birke and J.R. Lombardi, *Phys. Rev. Lett.* **43** (1979) 71.
27. M.W. Howard, R.P. Cooney and A.J. McQuillan, *J. Raman Spectrosc.* **9** (1980) 273.
28. M.R. Mahoney, M.W. Howard and R.P. Cooney, *Chem. Phys. Lett.* **71** (1980) 59.
29. R.P. Cooney, M.R. Mahoney and M.W. Howard, *Chem. Phys. Lett.* **76** (1980) 448.
30. J.C. Tsang, J.E. Demuth, P.N. Sanda and J.R. Kirtley, *Chem. Phys. Lett.* **76** (1980) 54.
31. A. Kudelski and B. Pettinger, *Chem. Phys. Lett.* **321** (2000) 356.
32. A. Kudelski and B. Pettinger, *Chem. Phys. Lett.* **383** (2004) 76.
33. B. Pettinger and H. Wetzel, *Chem. Phys. Lett.* **78** (1981) 398.
34. B. Bozzini, G.P. De Gaudenzi and C. Mele, *J. Electroanal. Chem.* **570** (2004) 29.